AGU PUBLICATIONS

Geophysical Research Letters

RESEARCH LETTER
10.1002/2016GL067972

Key Points:
- New data set of TTL water and cirrus microphysical observations
- Ice nucleation, growth, and sedimentation are important limiting factors in dehydration
- Dehydration efficiency decreases with temperature below 200 K

Correspondence to:
A. W. Rollins,
Andrew.Rollins@noaa.gov

Citation:
Rollins, A. W., T. D. Thornberry, R. S. Gao, S. Woods, R. P. Lawson, T. P. Bui, E. J. Jensen, and D. W. Fahey (2016), Observational constraints on the efficiency of dehydration mechanisms in the tropical tropopause layer, *Geophys. Res. Lett., 43*, 2912–2918, doi:10.1002/2016GL067972.

Received 25 JAN 2016
Accepted 29 FEB 2016
Accepted article online 6 MAR 2016
Published online 19 MAR 2016

Observational constraints on the efficiency of dehydration mechanisms in the tropical tropopause layer

A. W. Rollins[1,2], T. D. Thornberry[1,2], R. S. Gao[1], S. Woods[3], R. P. Lawson[3], T. P. Bui[4], E. J. Jensen[4], and D. W. Fahey[1,2]

[1]NOAA Earth System Research Laboratory, Boulder, Colorado, USA, [2]Cooperative Institute for Research in Environmental Sciences, University of Colorado Boulder, Boulder, Colorado, USA, [3]SPEC Inc., Boulder, Colorado, USA, [4]NASA Ames Research Center, Moffett Field, California, USA

Abstract The efficiency of dehydration in the tropical tropopause layer (TTL) determines how closely water vapor will be reduced to the lowest saturation mixing ratio encountered along a trajectory to the stratosphere, thereby strongly influencing stratospheric humidity. The NASA Airborne Tropical Tropopause Experiment (ATTREX) provided an unprecedented number and quality of in situ observations to constrain the key mechanisms controlling this dehydration. Statistical analyses of the ATTREX data show that nucleation, growth, and sedimentation each result in TTL dehydration becoming increasingly inefficient at temperatures below 200 K. Because of these inefficiencies, models that ignore these mechanisms likely underestimate water vapor at the stratospheric entry point by ~10–20% at the lowest temperatures.

1. Introduction

Water vapor (WV) is an important greenhouse gas. Radiative transfer calculations show that relative to the total atmospheric column, the small mass of WV in the lower stratosphere (SWV) plays a disproportionately significant role in controlling surface temperatures [*Forster and Shine*, 2002; *Solomon et al.*, 2010; *Riese et al.*, 2012].

The formation of cirrus clouds in the tropical tropopause layer (TTL, ~13–19 km) is the dominant process in regulating SWV. As air rises through this region of the atmosphere en route to the stratosphere, it experiences temperature minima where the humidity is frequently at or above saturation with respect to ice (i.e., $RH_i \geq 100\%$). When the humidity becomes high enough, cirrus clouds form, and the ice crystals grow and sediment, reducing the water content of an air parcel (i.e., dehydration) to a minimum before entering the stratosphere. Tight correlations between TTL temperatures and SWV have long suggested that the TTL dehydration process overwhelmingly controls SWV [e.g., *Randel et al.*, 2004; *Rosenlof and Reid*, 2008].

Because the microphysics of dehydration does not lead to instantaneous removal of all water in excess of saturation, the dehydration process is inherently inefficient; i.e., dehydration does not bring SWV as low as it would be if RH_i were always limited to 100%. Quantifying the details that control the efficiency of the dehydration process has been elusive. Both infrequent sampling of the key regions of the atmosphere and potential inaccuracies in water vapor measurements [*Fahey et al.*, 2014; *Rollins et al.*, 2014] and in ice crystal concentrations [*Jensen et al.*, 2009] have made it challenging to confidently evaluate cirrus cloud microphysical mechanisms using aircraft data [see *Krämer et al.*, 2009].

A recent series of research flights in the TTL using the NASA Global Hawk (GH) Unmanned Aircraft System during the NASA Airborne Tropical Tropopause Experiment (ATTREX) has provided an unprecedented set of aircraft observations of TTL water vapor and cirrus above the tropical Pacific. Here we use this data set to statistically evaluate and constrain the efficiency of the microphysical aspects of the dehydration process in the TTL.

2. Experimental

Research flights using the GH based at Armstrong Flight Research Center, California, were conducted in February–March 2013, and from Guam during February–March 2014 (Figure 1) [also see *Jensen et al.*, 2016]. The long endurance of the GH is allowed for transit to and from the tropics in addition to substantial vertical profiling in the TTL on each flight based at Armstrong. Flights based in Guam sampled exclusively in the tropics above the Western Pacific. Once in the tropics, the sampling strategy was generally to navigate the aircraft toward regions where clouds were anticipated based on temperature forecasts. In these regions the GH profiled

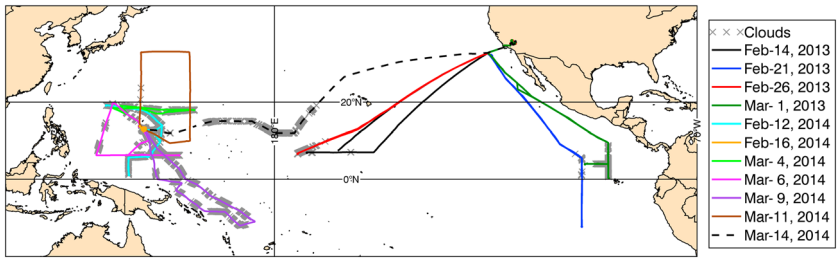

Figure 1. Global Hawk flight tracks and locations of cirrus measurements from boreal winters of 2013 and 2014. Grey symbols along flight tracks indicate both FCDP and NOAA IWC above detection limits.

vertically from near 14.5 km altitude to the maximum altitude of the aircraft (16–19 km, increasing throughout the flight duration). Due to GH operational limitations, the lowest temperatures were intentionally avoided, resulting in relatively limited sampling in regions colder than 186 K.

The GH carried instruments to measure water, ice crystal size distributions, and meteorological parameters. The NOAA-H_2O instrument is a two-channel tunable diode laser-based hygrometer housed inside the GH fuselage that samples WV into one channel using a sideways-facing inlet and enhanced total water (condensed phase water enhanced by a factor of ~30–50 plus WV) into a second channel using a forward-facing inlet [*Thornberry et al.*, 2014]. Periodic in situ calibrations (typically every 1–2 h) were used to verify the accuracy of the NOAA-H_2O measurements, which have total uncertainty (1σ) of $\pm(5\% + 0.23)$ ppm. Ice water content (IWC) was calculated from the enhanced total water and WV data by assuming a particle size-independent aspiration efficiency. Based on the observed particle size distributions, the IWC error is $<$2% for 95% of the observations. Larger errors occur for clouds dominated by very small crystals (~2–5 μm) [see *Thornberry et al.,* 2014], but these outliers do not significantly affect the analysis here. A Fast Cloud Droplet Probe (FCDP) provided number concentrations and sizing information for ice crystals between 1 and 50 μm in diameter [*O'Connor et al.*, 2008; *Lance et al.*, 2010]. In addition, during 2014 a Hawkeye instrument (SPEC Inc.) was added to the payload. The 2-D-Stereo (2D-S) portion of the Hawkeye provided this information for ice crystals from 10 μm up to ~3 mm [*Lawson et al.*, 2006]. The NASA Ames Meteorological Measurement System (MMS) [*Scott et al.*, 1990] provided the temperature and pressure data used here.

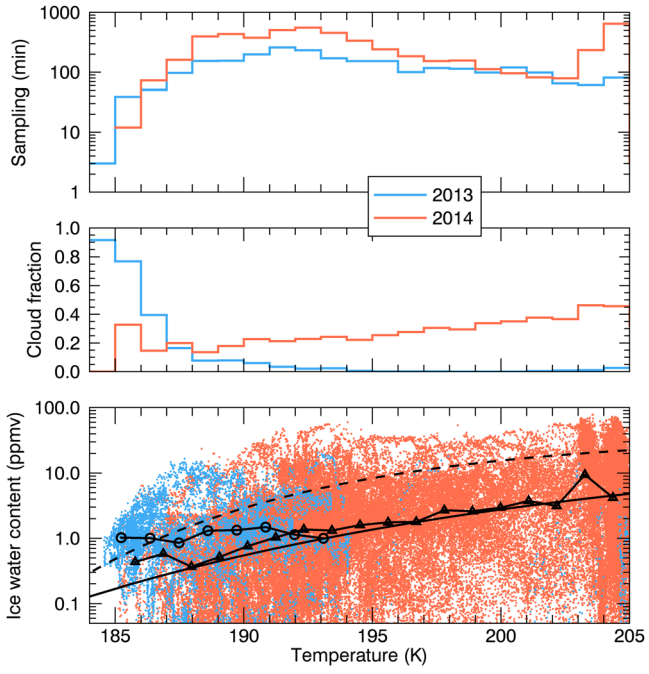

Figure 2. Blue = 2013. Red = 2014. (top) Minutes of tropical sampling. (middle) Fraction of observations where clouds were detected. (bottom) 1 Hz observations of ice water content. Dashed line shows the Schiller et al. parameterization; solid line shows the Schiller et al. "no convection" parameterization; circles show ATTREX 2013 average; and triangles show ATTREX 2014 average.

3. Observations

Cirrus clouds were frequently encountered in the tropics (12°S–20°N), with a total of 37 h of sampling within cirrus. Cirrus is defined here as a nonzero FCDP count rate for a 3 s running average and IWC above the detection limit (typically near 0.015 ppm).

Figure 2 shows the temperature and cloud frequency statistics for the ATTREX tropical sampling. The temperature statistics shown in Figure 2 are not necessarily representative of the frequency of occurrence of these temperatures in this region and were

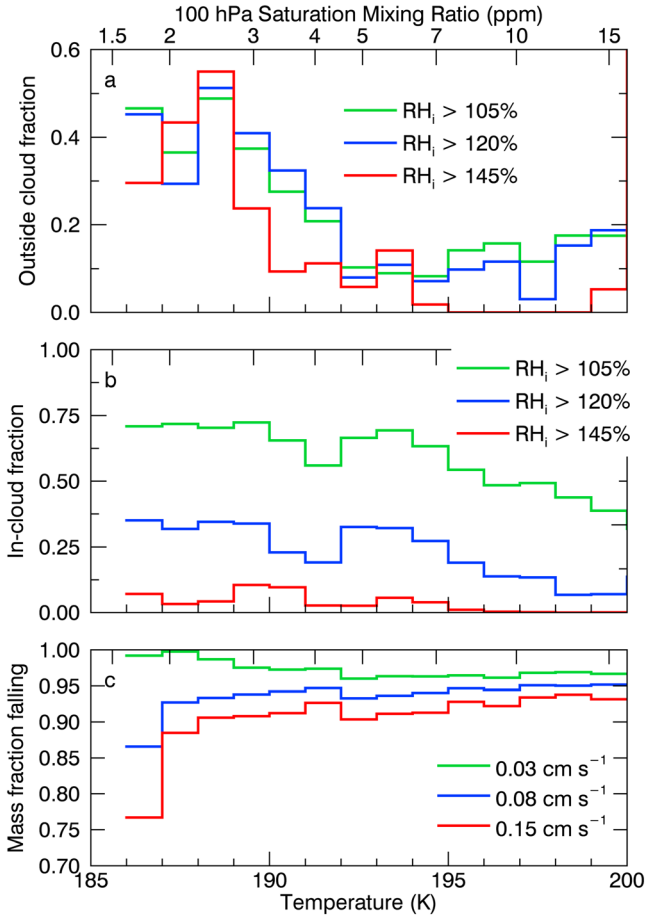

Figure 3. (a) Fraction of the supersaturated observations that were outside of clouds, and (b) fraction of clouds that were supersaturated for three RH_i threshold values. (c) IWC mass fraction with net downward flux assuming various ascent rates.

somewhat biased high by aircraft operations as described above. Differences between the 2013 and 2014 observations are most likely due to the different influences of deep convection between the Eastern (2013) and Western Pacific (2014) regions. Few measurements (<1 h) at temperatures below 186 K were made for the combined 2 years. Nonetheless, the average IWC versus temperature relationship reported here is quite similar to that reported by *Schiller et al.* [2008] for the tropics [see also *Luebke et al.*, 2013], providing evidence that both studies likely sampled cirrus that are representative of the climatology of tropical cirrus at 186 K and above.

4. Analysis

Dehydration of stratosphere-bound air is a process involving three microphysical mechanisms: (1) ice nucleation, (2) ice crystal growth, and (3) gravitational sedimentation. Here we analyze the ATTREX data to statistically constrain how each of these mechanisms affects the efficiency of TTL dehydration.

4.1. Ice Nucleation

The relative importance of different ice nucleation mechanisms in the upper troposphere is the subject of an ongoing debate involving measurements of the chemical composition of ice residuals [*Froyd et al.*, 2010; *Cziczo et al.*, 2013] as well as theoretical studies using ice concentration data [e.g., *Spichtinger and Krämer*, 2013; *Murphy*, 2014; *Dinh et al.*, 2016] but is not addressed in this analysis. The question we seek to address here is to what degree nucleation appears to be a limiting factor in dehydration. To answer this, we assume to first order that inside of a cloud, nucleation is not the limiting factor in gas to particle conversion of WV, while the opposite is true for supersaturated regions outside of clouds.

Figure 3a shows the fraction of supersaturated observations that occurred outside of clouds as a function of temperature using RH_i thresholds of 105%, 120%, and 145%. For all thresholds, at temperatures above 192 K only about 15% of supersaturated air parcels are cloud free; and hence, the majority of supersaturated air is inside of clouds. As temperatures decrease below 192 K, the fraction of supersaturated air parcels that remain cloud free increases, up to as much as ~50% near 186–187 K. These observations may suggest that ice nucleation typically occurs at a lower RH_i at the higher temperatures (>192 K). Such a limiting trend might be anticipated due simply to the temperature dependence of the homogeneous nucleation threshold [*Koop et al.*, 2000]; however, that theory would predict a less steep trend with higher RH_i thresholds. Another possibility is that heterogeneous nucleation at RH_i close to 100% is more prevalent at the higher temperatures, possibly due to activation and removal of the most effective ice nuclei prior to air parcels experiencing the lowest temperatures. This conclusion would be consistent with *Froyd et al.* [2010] and *Cziczo et al.* [2013], who use the chemical composition of sublimated ice residuals to argue for the importance of distinctly different ice nucleation mechanisms above and below 200 K. While *Cziczo et al.* [2013] show that

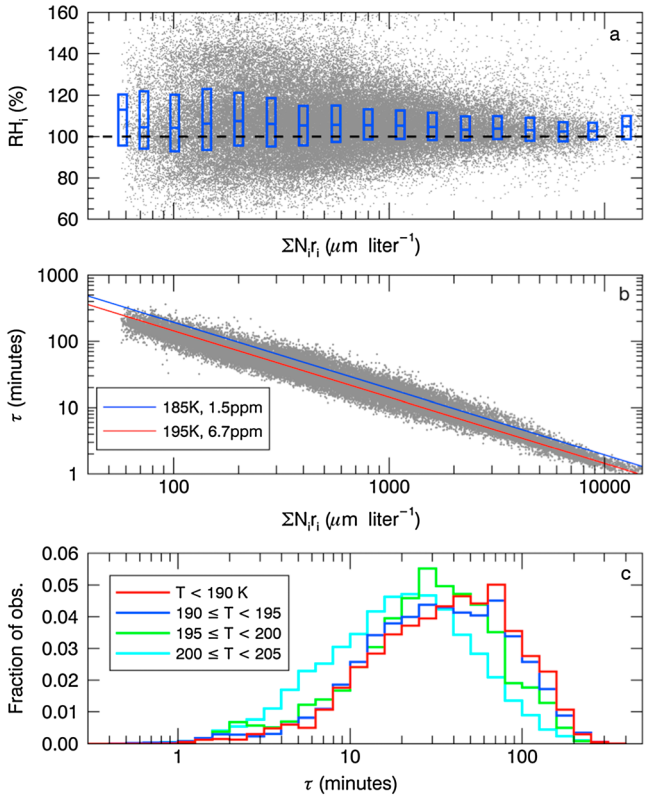

Figure 4. (a) Observed relationship between RH_i and $\Sigma N_i r_i$. Gray dots show 1 s data; boxes show median and interquartile range. (b) Calculated τ_p values using 1 Hz observations of *T*, *p*, WV, and $\Sigma N_i r_i$ (gray dots) and two example calculations at 120 hPa. (c) Distribution of calculated τ_p values from Figure 4b.

between ~200 and 240 K ice nucleation is dominated by mineral dust, *Froyd et al.* [2010] show that between 185 and 200 K the ice residuals are almost exclusively composed of sulfate and organic material.

4.2. Depositional Growth

In air parcels containing cirrus, exchange of WV between the gas and solid phases via depositional growth and sublimation results in RH_i tending toward an equilibrium value of 100%. The equilibrium relaxation time for TTL conditions is frequently comparable to the time air parcels spend at the lowest temperatures, which is highly variable due to wave activity [e.g., *Jensen and Pfister*, 2004]. As a result, the wide distribution of observed RH_i inside of clouds indicates that the kinetics of ice crystal growth is frequently an important factor controlling the efficiency of dehydration.

The frequency of observed cloud supersaturation is examined in Figure 3b, also using RH_i thresholds of 105%, 120%, and 145%. At temperatures below 200 K, supersaturation inside of clouds became increasingly frequent with decreasing temperature. An explanation for these observations derives from considering the gas/particle equilibrium time scale. The effectiveness of supersaturated clouds to deplete vapor through deposition onto ice crystals increases with ice concentration and size. The overall time scale for this mechanism (τ_p) in slowly ascending clouds primarily depends on the inverse of the integrated particle radius, $\Sigma N_i r_i$, where N_i is the number concentration of particles with radius r_i [*Korolev and Mazin*, 2003] and to a lesser extent on temperature, pressure, and humidity. Therefore, following ice crystal nucleation, in-cloud supersaturated conditions persist for long time periods when $\Sigma N_i r_i$ is relatively small.

Figure 4a shows the observed relationship between in-cloud RH_i and $\Sigma N_i r_i$. The mass-weighted average particle radius used in calculating the abscissa in Figure 4a was derived using IWC and FCDP number concentration data assuming spherical ice crystals with a density (ρ_i) of 0.92 g cm^{-3}. This average radius was then multiplied by the FCDP number concentration to arrive at $\Sigma N_i r_i$. As a check, $\Sigma N_i r_i$ was also calculated by (1) using only the FCDP size distributions assuming ice crystals with diameter equal to the middle of each bin and (2) using a combination of FCDP and 2D-S size distributions (FCDP up to 24 μm and 2D-S above 25 μm). These calculations demonstrated that all three methods generally agree within 20%, and using the measured IWC is advantageous for this analysis because it provides $\Sigma N_i r_i$ values without the discretization resulting from the size binning of the crystal probes. The disadvantage of this method is that the lowest $\Sigma N_i r_i$ may be omitted due the IWC detection limit.

Figure 4a shows the 1 s RH_i versus $\Sigma N_i r_i$ observations and statistics with the median and interquartile. Figure 4b shows calculations of τ_p as a function of $\Sigma N_i r_i$, using the formulation of *Korolev and Mazin* [2003]. These data show a consistent relationship of increased RH_i variability as τ_p increases and $\Sigma N_i r_i$ decreases. At the highest $\Sigma N_i r_i$ values (~10,000 μm L^{-1}) the interquartile range spans an 11% RH_i range, whereas for the most frequent $\Sigma N_i r_i$ (~500 μm L^{-1}), it is 20%. The largest range is 29% near 150 μm L^{-1}. The distribution width at the highest $\Sigma N_i r_i$ values is close to that expected due solely to the precision of the WV measurement (σ = 0.17 ppm, interquartile range = 0.23 ppm). Figure 4c shows histograms of the calculated τ_p values from Figure 4b, demonstrating that

relaxation times of 10 min to 1 h were frequent in the TTL with the longest τ_p being more frequent at the lowest temperatures. These calculations agree well with those by *Krämer et al.* [2009] for cirrus at temperatures below 200 K. Many of the very thinnest clouds ($\Sigma N_i r_i < 100\ \mu m\ L^{-1}$) were observed at the bases of denser clouds. The sampled ice crystals in those locations are thought to be sublimating ice crystals that were sedimenting from higher clouds, explaining the decreasing RH_i trend at the lowest $\Sigma N_i r_i$.

4.3. Ice Sedimentation

Gravitational sedimentation of ice crystals ultimately removes H_2O from ascending air. Since the large-scale motion of air in the TTL is upward, ice formation will only lead to a net downward flux of H_2O if the ice is falling faster than the local ascent rate. Even if the ice sedimentation speed is a significant fraction of the ascent rate, resulting in dehydration of the local airmass, unless the ice has a net negative vertical velocity, the condensed H_2O is still being transported toward the stratosphere. To reduce total water to the lowest RH_i experienced by an air parcel, ice crystals must be removed rapidly enough to leave an air parcel during the periods when the lowest temperatures are experienced, which will sometimes be quite transient due to wave activity. Local TTL ascent rates are challenging to constrain but are thought to be in the range of 0.02–0.1 cm s^{-1}. Ice crystal fall speeds may be slower than the fastest ascent rates. For example, assuming spherical ice with $\rho_i = 0.92$ g cm^{-3} at 100 hPa and 200 K, the calculated terminal velocity is 0.1 cm s^{-1} for a 5 μm particle; and thus, smaller crystals will fall more slowly than 0.1 cm s^{-1}.

To evaluate how sedimentation limits dehydration, we calculated the fraction of IWC sedimenting out of air parcels sampled during ATTREX using the fall speeds of individual crystals calculated with FCDP size distributions and MMS temperature and pressure measurements, and assuming spherical ice with $\rho_i = 0.92$ g cm^{-3}. Using these fall speeds and sizes of crystals for each 1 s measurement, the fractions of IWC falling faster than assumed ascent rates of 0.03, 0.08, and 0.15 cm s^{-1} were calculated, and the ATTREX average fraction was plotted as a function of temperature (Figure 3c). Due to the ubiquity of very small ice crystals, the fraction of IWC falling is 0.95 or less for many of the air parcels encountered. With ascent rates of 0.08 and 0.15 cm s^{-1} a trend of decreasing sedimentation efficiency at lower temperatures is observed due to the prevalence of ice crystals in the 3–6 μm range.

5. Discussion

The analyses presented here provide evidence from in situ sampling that the TTL dehydration process becomes increasingly inefficient as temperature decreases below 200 K. The temperature dependences shown in Figure 3 are previously unreported but nonetheless are consistent with cirrus microphysical models. For example, the in-cloud supersaturations can be reasonably explained as a kinetic effect assuming that hexagonal ice is the sole solid phase (Figure 4). The results presented here and by *Krämer et al.* [2009] are a major step forward considering that within the past decade the basic physical principles controlling cirrus clouds have been drawn into question due to disagreements between observations and theory [*Peter et al.*, 2006].

Figure 3a suggests that the supersaturation required for nucleation may limit dehydration efficiency at temperatures below 195 K to no more than ~90% (i.e., more than 10% of the time, nucleation does not occur in supersaturated air parcels). However, without making assumptions about the temperature fields that will be experienced in the future by the air parcels similar to those that were sampled, it is difficult to confidently draw quantitative and representative conclusions. If, for example, temperature fluctuations were completely stochastic due to large numbers of randomly phased waves, Figures 3a and 3b could be assumed to be reasonable quantifications of the typical efficiencies of nucleation and growth because it would be just as likely for RH_i to increase or decrease following each observation. If, however, the updrafts determining the TTL temperature variability are more coherent, then many of the air parcels contributing to Figure 3a will continue to cool and eventually nucleate, making the statistics shown here a lower limit to dehydration efficiency.

The sedimentation fraction calculations shown in Figure 3c quantify an important constraint on dehydration efficiency. These calculations show an upper limit to how effectively sedimenting ice crystals remove ice in the TTL at any given time. Sedimentation effectiveness is fundamentally sensitive to the local ascent rates. These rates are somewhat uncertain, though the values for the mean TTL ascent rate derived using multiple approaches lie mostly near 0.03–0.04 cm s^{-1} [*Schoeberl et al.*, 2008; *Park et al.*, 2010; *Ploeger et al.*, 2010]. In Boreal winter (ATTREX time frame), the ascent is somewhat faster than the annual average (~0.06 cm s^{-1})

[*Randel et al.*, 2008]. Additionally, in air containing ice crystals, the local ascent rate due to absorption of radiation by the clouds is significantly higher than in cloud-free regions [*Jensen et al.*, 1996; *Corti et al.*, 2006; *Dinh and Fueglistaler*, 2014]. For example, *Corti et al.* [2006] show that in TTL clouds, the net radiative heating rate distribution peaks near 2 K d^{-1}, which is 4 times the average TTL heating rate. Thus, in cloudy regions during Boreal winter the ascent rate may be 0.1 cm s^{-1} or greater; and therefore, 10% or more of the mass of ice formed may continue to ascent toward the stratosphere (Figure 3c). Even for the ice falling faster than the local ascent rate, most of it will clearly be falling at a very slow rate, which implies the cirrus will be long lived and therefore radiatively important.

The trends shown in Figure 3 provide powerful constraints on model calculations of TTL dehydration and SWV. TTL dehydration efficiency clearly decreases with temperature below 200 K for fundamental physical reasons. This temperature dependence of the dehydration efficiency will further enhance the nonlinear relationship between TTL temperatures and SWV, beyond that due to the vapor pressure of ice. This can be used as a diagnostic for models that calculate stratospheric water vapor by including the microphysical mechanisms important for the dehydration process. Because the very coldest clouds in the TTL necessarily result in the driest air and are the final dehydration points for many stratosphere-bound air parcels, future missions should focus on unbiased sampling of these coldest clouds to evaluate to what degree the dehydration efficiency continues to decrease below 186 K.

Acknowledgments
We thank the Armstrong Flight Research Center Global Hawk crew and pilots for making these measurements possible. This research was funded by the NOAA Atmospheric Chemistry, Carbon Cycle, and Climate Program, the NASA Airborne Tropical Tropopause Experiment, and the NASA Radiation Sciences Program. Data used in this analysis are archived by NASA (https://espoarchive.nasa.gov/archive/browse/attrex).

References

Corti, T., B. P. Luo, Q. Fu, H. Vömel, and T. Peter (2006), The impact of cirrus clouds on tropical troposphere-to-stratosphere transport, *Atmos. Chem. Phys.*, *6*(9), 2539–2547, doi:10.5194/acp-6-2539-2006.

Cziczo, D. J., K. D. Froyd, C. Hoose, E. J. Jensen, M. Diao, M. A. Zondlo, J. B. Smith, C. H. Twohy, and D. M. Murphy (2013), Clarifying the dominant sources and mechanisms of cirrus cloud formation, *Science*, *340*(6138), 1320–1324, doi:10.1126/science.1234145.

Dinh, T., and S. Fueglistaler (2014), Microphysical, radiative, and dynamical impacts of thin cirrus clouds on humidity in the tropical tropopause layer and lower stratosphere, *Geophys. Res. Lett.*, *41*, 6949–6955, doi:10.1002/2014GL061289.

Dinh, T., A. Podglajen, A. Hertzog, B. Legras, and R. Plougonven (2016), Effect of gravity wave temperature fluctuations on homogeneous ice nucleation in the tropical tropopause layer, *Atmos. Chem. Phys.*, *16*(1), 35–46, doi:10.5194/acp-16-35-2016.

Fahey, D. W., et al. (2014), The AquaVIT-1 intercomparison of atmospheric water vapor measurement techniques, *Atmos. Meas. Tech.*, *7*(9), 3177–3213, doi:10.5194/amt-7-3177-2014.

Forster, P. M. D. F., and K. P. Shine (2002), Assessing the climate impact of trends in stratospheric water vapor, *Geophys. Res. Lett.*, *29*(6), 1086, doi:10.1029/2001GL013909.

Froyd, K. D., D. M. Murphy, P. Lawson, D. Baumgardner, and R. L. Herman (2010), Aerosols that form subvisible cirrus at the tropical tropopause, *Atmos. Chem. Phys.*, *10*(1), 209–218, doi:10.5194/acp-10-209-2010.

Jensen, E. J., and L. Pfister (2004), Transport and freeze-drying in the tropical tropopause layer, *J. Geophys. Res.*, *109*, D02207, doi:10.1029/2003JD004022.

Jensen, E. J., O. B. Toon, H. B. Selkirk, J. D. Spinhirne, and M. R. Schoeberl (1996), On the formation and persistence of subvisible cirrus clouds near the tropical tropopause, *J. Geophys. Res.*, *101*(D16), 21,361–21,375, doi:10.1029/95JD03575.

Jensen, E. J., et al. (2009), On the importance of small ice crystals in tropical anvil cirrus, *Atmos. Chem. Phys.*, *9*, 5519–5537, doi:10.5194/acp-9-5519-2009.

Jensen, E. J., et al. (2016), The NASA Airborne Tropical TRopopause EXperiment (ATTREX): High-altitude aircraft measurements in the tropical western Pacific, *Bull. Am. Meteorol. Soc.*, doi:10.1175/BAMS-D-14-00263.1, in press.

Koop, T., B. Luo, A. Tsias, and T. Peter (2000), Water activity as the determinant for homogeneous ice nucleation in aqueous solutions, *Nature*, *406*(6796), 611–614, doi:10.1038/35020537.

Korolev, A. V., and I. P. Mazin (2003), Supersaturation of water vapor in clouds, *J. Atmos. Sci.*, *60*(24), 2957–2974, doi:10.1175/1520-0469(2003)060<2957:SOWVIC>2.0.CO;2.

Krämer, M., et al. (2009), Ice supersaturations and cirrus cloud crystal numbers, *Atmos. Chem. Phys.*, *9*(11), 3505–3522, doi:10.5194/acp-9-3505-2009.

Lance, S., C. A. Brock, D. Rogers, and J. A. Gordon (2010), Water droplet calibration of the Cloud Droplet Probe (CDP) and in-flight performance in liquid, ice and mixed-phase clouds during ARCPAC, *Atmos. Meas. Tech.*, *3*(6), 1683–1706, doi:10.5194/amt-3-1683-2010.

Lawson, R. P., D. O'Connor, P. Zmarzly, K. Weaver, B. Baker, Q. Mo, and H. Jonsson (2006), The 2D-S (Stereo) probe: Design and preliminary tests of a new airborne, high-speed, high-resolution particle imaging probe, *J. Atmos. Oceanic Technol.*, *23*(11), 1462–1477, doi:10.1175/JTECH1927.1.

Luebke, A. E., L. M. Avallone, C. Schiller, J. Meyer, C. Rolf, and M. Krämer (2013), Ice water content of Arctic, midlatitude, and tropical cirrus—Part 2: Extension of the database and new statistical analysis, *Atmos. Chem. Phys.*, *13*(13), 6447–6459, doi:10.5194/acp-13-6447-2013.

Murphy, D. M. (2014), Rare temperature histories and cirrus ice number density in a parcel and a one-dimensional model, *Atmos. Chem. Phys.*, *14*(23), 13,013–13,022, doi:10.5194/acp-14-13013-2014.

O'Connor, D., B. Baker, and R. P. Lawson (2008), Upgrades to the FSSP-100 Electronics, p. 13.6, 15th International Conference on Clouds and Precipitation, Cancun, Mexico.

Park, S., et al. (2010), Vertical transport rates and concentrations of OH and Cl radicals in the tropical tropopause Layer from observations of CO_2 and halocarbons: Implications for distributions of long- and short-lived chemical species, *Atmos. Chem. Phys.*, *10*(14), 6669–6684, doi:10.5194/acp-10-6669-2010.

Peter, T., C. Marcolli, P. Spichtinger, T. Corti, M. B. Baker, and T. Koop (2006), When dry air is too humid, *Science*, *314*(5804), 1399–1402, doi:10.1126/science.1135199.

Ploeger, F., P. Konopka, G. Günther, J.-U. Grooß, and R. Müller (2010), Impact of the vertical velocity scheme on modeling transport in the tropical tropopause layer, *J. Geophys. Res.*, *115*, D03301, doi:10.1029/2009JD012023.

Randel, W. J., F. Wu, S. J. Oltmans, K. Rosenlof, and G. E. Nedoluha (2004), Interannual changes of stratospheric water vapor and correlations with tropical tropopause temperatures, *J. Atmos. Sci.*, *61*(17), 2133–2148, doi:10.1175/1520-0469(2004)061<2133:ICOSWV>2.0.CO;2.

Randel, W. J., R. Garcia, and F. Wu (2008), Dynamical balances and tropical stratospheric upwelling, *J. Atmos. Sci.*, *65*(11), 3584–3595, doi:10.1175/2008JAS2756.1.

Riese, M., F. Ploeger, A. Rap, B. Vogel, P. Konopka, M. Dameris, and P. Forster (2012), Impact of uncertainties in atmospheric mixing on simulated UTLS composition and related radiative effects, *J. Geophys. Res.*, *117*, D16305, doi:10.1029/2012JD017751.

Rollins, A. W., et al. (2014), Evaluation of UT/LS hygrometer accuracy by intercomparison during the NASA MACPEX mission, *J. Geophys. Res. Atmos.*, *119*, 1915–1935, doi:10.1002/2013JD020817.

Rosenlof, K. H., and G. C. Reid (2008), Trends in the temperature and water vapor content of the tropical lower stratosphere: Sea surface connection, *J. Geophys. Res.*, *113*, D06107, doi:10.1029/2007JD009109.

Schiller, C., M. Krämer, A. Afchine, N. Spelten, and N. Sitnikov (2008), Ice water content of Arctic, midlatitude, and tropical cirrus, *J. Geophys. Res.*, *113*, D24208, doi:10.1029/2008JD010342.

Schoeberl, M. R., A. R. Douglass, R. S. Stolarski, S. Pawson, S. E. Strahan, and W. Read (2008), Comparison of lower stratospheric tropical mean vertical velocities, *J. Geophys. Res.*, *113*, D24109, doi:10.1029/2008JD010221.

Scott, S. G., T. P. Bui, K. R. Chan, and S. W. Bowen (1990), The Meteorological Measurement System on the NASA ER-2 Aircraft, *J. Atmos. Oceanic Technol.*, *7*(4), 525–540, doi:10.1175/1520-0426(1990)007<0525:TMMSOT>2.0.CO;2.

Solomon, S., K. H. Rosenlof, R. W. Portmann, J. S. Daniel, S. M. Davis, T. J. Sanford, and G.-K. Plattner (2010), Contributions of stratospheric water vapor to decadal changes in the rate of global warming, *Science*, *327*(5970), 1219–1223, doi:10.1126/science.1182488.

Spichtinger, P., and M. Krämer (2013), Tropical tropopause ice clouds: A dynamic approach to the mystery of low crystal numbers, *Atmos. Chem. Phys.*, *13*(19), 9801–9818, doi:10.5194/acp-13-9801-2013.

Thornberry, T. D., A. W. Rollins, R. S. Gao, L. A. Watts, S. J. Ciciora, R. J. McLaughlin, and D. W. Fahey (2014), A two-channel, tunable diode laser-based hygrometer for measurement of water vapor and cirrus cloud ice water content in the upper troposphere and lower stratosphere, *Atmos. Meas. Tech.*, *8*(1), 211–224, doi:10.5194/amt-8-211-2015.